

Article

Slag and Activator Chemistry Control the Reaction Kinetics of Sodium Metasilicate-Activated Slag Cements

Maria Criado^{1,2}, Brant Walkley¹, Xinyuan Ke^{1,3} , John L. Provis^{1,*}  and Susan A. Bernal^{1,4,*}

¹ Department of Materials Science and Engineering, The University of Sheffield, Sir Robert Hadfield Building, Sheffield S1 3JD, UK; maria.criado@ietcc.csic.es (M.C.); b.walkley@sheffield.ac.uk (B.W.); x.ke@bath.ac.uk (X.K.)

² Eduardo Torroja Institute for Construction Sciences (IETcc-CSIC), Madrid 28033, Spain

³ BRE Centre for Innovative Construction Materials, University of Bath, Bath BA2 7AY, UK

⁴ School of Civil Engineering, University of Leeds, Woodhouse Lane, Leeds LS2 9JT, UK

* Correspondence: j.provis@sheffield.ac.uk (J.L.P.); S.A.BernalLopez@leeds.ac.uk (S.A.B.)

Received: 11 September 2018; Accepted: 7 December 2018; Published: 11 December 2018



Abstract: The reaction kinetics of four commercial ground granulated blast furnace slags with varying percentages of MgO (6 to 14 wt.%), activated with four different doses of sodium metasilicate, were evaluated using isothermal calorimetry. The reaction kinetics were strongly dependent on the dose of the alkaline activator used, and the chemical and physical properties of the slag. When using low concentrations of sodium metasilicate as an activator, the MgO content in the slag influences the kinetics of the reaction, while the CaO content plays a more significant role when the concentration of metasilicate is increased. This study elucidated a close relationship between the dose of the alkali-activator and the chemistry of the slag used, although it was not possible to identify a clear correlation between any of the published chemically-based “slag quality moduli” and the calorimetry results, highlighting the complexity of blast furnace slag glass chemistry, and the importance of the physical properties of the slag in defining its reactivity.

Keywords: alkali-activated cements; isothermal calorimetry; slag chemistry; sodium metasilicate

1. Introduction

There have recently been extensive efforts by industry and academia to improve the sustainability of concrete production, and a key focus has been the partial or complete replacement of Portland cement (PC) clinker with supplementary cementitious materials [1]. In the case of the complete replacement of Portland cement by granulated blast furnace slag (GBFS, hereafter referred to as slag), highly alkaline solutions including caustic alkalis or alkaline salts are required to promote the reactions that lead to the formation of hardened products [2–4]. The cements formed by this process are commonly referred to as alkali-activated slag cements. The reactivity of slag in an alkaline solution is governed by its mineralogical and chemical composition, fineness and particle size distribution as well as the type and concentration of the alkaline solution used [5]. The addition of alkalis promotes slag dissolution and the formation of reaction products, primarily calcium silicate hydrates that incorporate significant amounts of aluminum (C-(A)-S-H), and additional reaction products such as layered double hydroxide (LDH) phases exhibiting hydrotalcite-group structures with Mg/Al ratios between 2 and 3 [6–8], and/or zeolite phases, depending on the slag chemistry [9].

Most studies of alkali-activated cements aim to understand how different activation conditions influence their phase assemblage and mechanical strength development, but few have been dedicated

to elucidating the influence of changes in raw material chemistry on the kinetics of reaction. The typical approach used to evaluate these cements is based on identifying optimized activation conditions for a given precursor, mainly considering mechanical strength performance. However, the fresh state properties of these cements, particularly setting time, will largely determine the most suitable application of these materials (e.g., pre-casting or on-site casting). Due to the vast number of parametric studies reporting varying setting times of these cements under different formulation, mixing, and curing conditions, it is challenging to use the data available in the literature to draw any correlation between specific properties of slags, activation conditions, and reaction kinetics. Thus, the goal of the present study is to achieve this using a systematic approach to the alkali-activation of a set of slags with differing compositions.

Sodium silicate ($\text{Na}_2\text{O}\cdot r\text{SiO}_2$) and sodium hydroxide (NaOH) are some of the alkali solutions that are most widely used in producing alkali-activated slag cements [10]. The pH of the activating solution plays an important role in the initial dissolution and polycondensation of silicate and aluminate species in alkali-activated slag cements [11,12]; activating solutions with a high pH promote slag dissolution [13], while those with pH values lower than 9.5 do not facilitate the dissolution and reaction of the slag precursor [12]. When comparing the NaOH and $\text{Na}_2\text{O}\cdot r\text{SiO}_2$ solutions used to produce alkali-activated slag cements, similar degrees of reaction are observed in each system despite NaOH exhibiting a higher pH than the silicate solutions of corresponding alkali concentration. However, silicate-activated slag cements exhibit higher mechanical performance and stability than hydroxide-activated slag cements due to the nature of the reaction products formed [5].

Blast furnace slag glass comprises predominantly CaO, SiO_2 , MgO, and Al_2O_3 [14], and the varying contents of these oxides will affect the reaction mechanisms and kinetics during alkali activation. The influence of slag MgO and Al_2O_3 content on alkali activation reaction kinetics has gained significant interest; Bernal et al. [9] observed that an increase in MgO content (between 1.7 and 7.4 wt.%) resulted in slower kinetics of reaction in silicate-activated slag cements due to the formation of a hydrotalcite-group phase in addition to C-(A)-S-H. A correlation between higher slag MgO content (up to 13.4 wt.%) and a higher degree of reaction (particularly at an early age) in silicate-activated slag cements was also observed by Ben Haha et al. [15]. Conversely, no marked differences in the kinetics of reaction were observed among hydroxide-activated slags [15]. With a constant slag MgO content, an increased Al_2O_3 content reduced the rate of reaction during the first few days of curing for both hydroxide- and silicate-based activating solutions [16], although the mechanisms behind this are unclear. This effect was not observed at later ages. These studies identified a close correlation between slag MgO and Al_2O_3 availability, and the reaction kinetics of alkali-activated cements is significant partly because of the consumption of Mg and Al by the growth of hydrotalcite-group LDH phases that form as additional reaction products.

In this study, the influence of the slag chemistry and activator concentration on the kinetics of reaction of alkali-activated slag cements was determined using isothermal calorimetry. Various proposed slag quality coefficients, calculated according to previously-published formulae that consider the chemical composition of slag, were compared and correlated with the time of onset of the acceleration period, which is often related to the initial setting time of cementitious materials. This is used to identify whether these coefficients can be utilized as criteria for the formulation of alkali-activated slag cements with specific kinetics of reaction.

2. Experimental Methodology

2.1. Sample Preparation

Four commercial slags were used; their oxide compositions (as determined by X-ray fluorescence), Blaine fineness, and average particle size are shown in Table 1. Four formulations, each with a different dose (3, 5, 7, and 8 wt.% relative to the anhydrous slag) of sodium metasilicate (Na_2SiO_3 , $\text{SiO}_2/\text{Na}_2\text{O} = 1$), were produced using each slag to assess the effect of the amount of soluble silicates supplied by the

activator on the reaction kinetics. All pastes were formulated with a water/binder ratio = 0.40, where the definition of ‘binder’ includes the dissolved activator solids. For each formulation, the appropriate quantity of anhydrous sodium metasilicate was fully dissolved in distilled water, and this solution was then manually mixed with the anhydrous slag for 2–3 min until a homogenous paste was formed.

Table 1. Chemical composition (as determined by X-ray fluorescence analysis *) and the physical properties of the anhydrous slags.

Slag ID †	CaO	SiO ₂	Al ₂ O ₃	MgO	SO ₃	Fe ₂ O ₃	TiO ₂	MnO	K ₂ O	Others	LOI ‡	Blaine Fineness (m ² /kg)	d ₅₀ (μm) §
M06	41.8	36.0	11.3	6.5	0.7	0.3	0.5	0.3	0.4	0.3	2.0	506	11
M07	40.2	34.1	12.4	7.4	2.0	0.3	0.6	0.4	0.3	0.0	-0.6	444	12
M08	39.6	35.1	13.1	8.5	0.2	0.3	0.7	0.4	0.5	0.1	1.0	404	16
M14	33.9	37.4	8.9	14.3	0.7	0.4	0.4	1.0	0.5	0.4	1.9	480	14

* Chemical compositions for all elements are given as oxides and do not necessarily correspond to the oxidation state in the anhydrous slags, particularly for sulfur which is represented as SO₃, but is likely to be present in reduced redox states in the slags. † Slag IDs are assigned according to MgO content. ‡ LOI: Loss on ignition at 1000 °C.

§ Determined by laser diffraction using a dry dispersion unit.

2.2. Determination of Reaction Kinetics

Isothermal calorimetry experiments were conducted using a TAM Air isothermal calorimeter (TA Instruments, New Castle, DE, USA) at a temperature of 25 ± 0.02 °C. Fresh pastes were mixed externally (as described above) and then 20 g of each paste was transferred into an ampoule and immediately placed in the calorimeter to record heat flow for the first 120 h of reaction. All values of heat release rate were normalized by the total mass of the paste analyzed.

2.3. Thermodynamic Modeling of Phase Evolution

The phase assemblages of sodium metasilicate-activated slag M06, with activator doses of 3 wt.% and 7 wt.% respectively, were simulated via thermodynamic modeling. The method of Gibbs energy minimization was used to predict the stable phases that may be expected to form in the system during its reaction. The thermodynamic model for alkali-activated slag system developed by Myers et al. [17] was used as the general framework, and open source software GEM-Selektor v.3 (GEMS3) was used for performing the modeling. The Truesdell–Jones form of the extended Debye–Hückel equation was used to calculate the aqueous-phase activity coefficients, and solid solution models for alkali-substituted calcium aluminate silicate hydrate gels (CNASH_{ss}) and for hydroxylated hydrotalcite (MgAl-OH-LDH_{ss}) were used; these are all described in detail in [17,18].

For slag activated by 7 wt.% of activator, the degree of reaction in the simulations was set to be 61% at 72 h after mixing, adopted from the experimental observations in a previous study [19], where slag with a similar chemical composition was used. For slag activated by the 3 wt.% activator, the degree of reaction at 72 h was proportionally scaled down, based on the assumption that the total reaction heat was proportional to the degree of reaction. The evolution of the degree of reaction within the initial 72 h of reaction time was then scaled in proportion to the cumulative heat release at each time during the same time of reaction.

3. Results and Discussion

3.1. Influence of Slag Chemistry and Activator Dose in Reaction Kinetics

For all doses of the sodium metasilicate activator, the heat release curves (Figure 1) exhibited a pre-induction period (first peak) during the first hour of reaction, corresponding to wetting and dissolution of the slag grains [20], and possibly also to the adsorption of some ions onto the surface of the slag grains. The sodium metasilicate solution had a high concentration of partially-deprotonated monomeric silicate anions, which reacted rapidly with Ca²⁺ as it dissolved from the surface of slag grains, to form an aluminum substituted calcium silicate hydrate (C-(A)-S-H) type gel, when the

concentration of Ca^{2+} reached a critical value [11]. The identification of this pre-induction period is consistent with several previous observations of sodium silicate activated slag cements [8,11].

The pre-induction peak was followed by a period of low heat release and reduced reaction. The duration of this period is strongly dependent on both the slag composition and the activator dose. At the end of this period, high intensity acceleration and deceleration periods corresponding to the nucleation, growth, and precipitation of reaction products (second peak) were observed in all alkali-activated slag cements. This period took place between 7 h and 100 h after the start of the reaction (Figure 1), depending on the slag composition and the concentration of the sodium silicate used, indicating that the reaction kinetics in alkali-activated slag cements are strongly dependent on the cement mix design.

At the lowest sodium metasilicate concentration investigated (3 wt.%, Figure 1A), sample M06 (which contained the lowest MgO content of the reaction mixes assessed) exhibited the longest induction period of all samples, lasting 38.0 h, with the maximum heat release rate in the acceleration-deceleration period (i.e., the beginning of the deceleration period) observed 55.7 h after mixing. Increased slag MgO content resulted in a reduction in the length of the induction period to 26 h and 18.6 h in samples M08 and M14, respectively, and promoted faster precipitation of the reaction products, indicated by the earlier onset of the deceleration period at 42.1 h and 34.5 h for samples M08 and M14, respectively. This is consistent with previous observations that sodium metasilicate-activated slags with higher slag MgO content reacted more rapidly than those with lower MgO content [15].

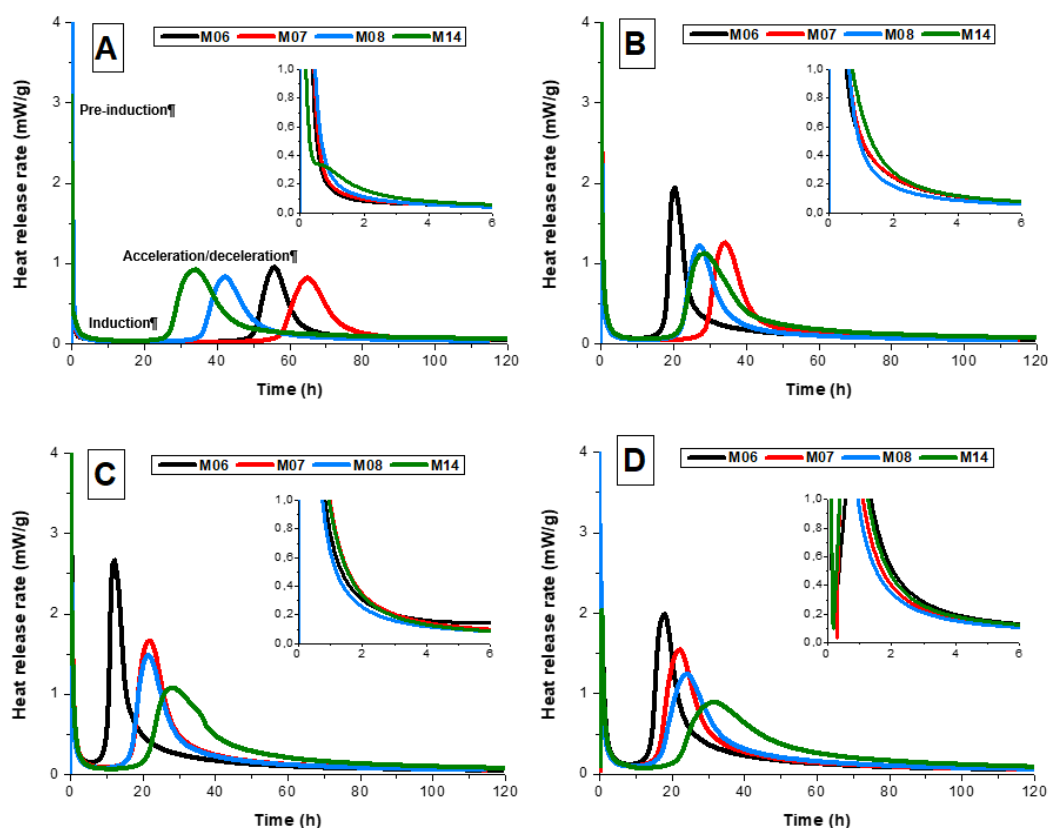


Figure 1. Heat release rate of sodium metasilicate activated slag cements produced with activator concentrations of (A) 3 wt.%, (B) 5 wt.%, (C) 7 wt.%, and (D) 8 wt.% (relative to mass of anhydrous slag), as a function of the slag chemistry. The different stages of the reaction process discussed in the text are indicated in (A).

Despite sample M07 having a higher MgO content than sample M06 (Table 1), its induction period was more prolonged (41.7 h) and its main reaction peak in Figure 1A was observed after 64.8 h. This behavior is likely to be related to an increased reactivity of the M06 slag, associated with a higher

specific area ($505.6 \text{ m}^2/\text{kg}$) and higher content of fine particles (d_{50} of $11.2 \text{ }\mu\text{m}$) when compared to the M07 slag. It is also possible that the higher content of sulfide (represented as SO_3 in the XRF data in Table 1, but usually present in reduced form in blast furnace slags) in M07 than M08 had some effect in retarding the reaction, considering that this was the most noticeable difference between M07 and M08, and the differences in particle size parameters were negligible. However, the presence of sulfide or other redox-active components is generally believed to increase, rather than decrease, the dissolution rates of solids [21], so it is not very clear how such a mechanism would take place from a chemical perspective.

Heat release curves for each slag activated with 5 wt.% sodium metasilicate are shown in Figure 1B. The increased activator dose resulted in a shorter duration induction period, an earlier onset of the acceleration/deceleration peak, and more intense heat release for all samples than at the lower activator dose in Figure 1A, indicating more rapid dissolution of the slag precursor and formation of reaction products. However, these changes did not occur to the same extent across all samples. The increased reaction kinetics observed were consistent with the higher concentration of soluble silicate supplied by the activator, which reacts with dissolved Ca^{2+} ions to remove them from the aqueous phase, thus increasing the Ca^{2+} concentration gradient between the pore solution and anhydrous slag grains. This drives faster dissolution of the slag particles and precipitation of mainly C-(A)-S-H type gels [11,22,23], which have been reported as the main reaction product for the silicate activated slags used in this study, and others of comparable composition [9]. Increased concentrations of soluble silicates will also reduce the degree of slag dissolution required to reach saturation in the aqueous phase relative to C-(A)-S-H, thus driving more rapid precipitation of the reaction products. Sample M06 exhibited the shortest induction period of the samples assessed, followed by sample M14 (despite its lower CaO content than the other slags), sample M08, and sample M07. This can mainly be attributed to the greater surface area of the slag used to produce sample M06 when compared with the other slags (Table 1), driving a more rapid reaction, although differences in slag chemistry will also influence this behavior as discussed in more detail below.

Increasing the concentration of sodium metasilicate to 7 wt.% (Figure 1C) slightly reduced the induction period for the M07 and M08 slags, compared with that observed when using 5 wt.% sodium metasilicate (Figure 1B). Sample M06 exhibited a sharper and more intense acceleration/deceleration peak than the other samples assessed at this activator dosage, and also compared to that observed when using lower activator doses (Figure 1A,B). Sample M14 exhibited the longest dormant period of the samples evaluated at this activator dosage as well as an acceleration/deceleration peak of lower intensity. Slag M14 had the lowest content of CaO of all the slags assessed, hence buffering the reaction for the preferential formation of C-A-S-H type phases over Mg-rich products. This behavior was also observed by Ben Haha et al. [8], who identified the delayed reaction of high-MgO slags when compared to slags with lower MgO content when using metasilicate as the activator at a relatively high dose (10 wt.%).

It is worth noting that for sample M14, the onset of the acceleration/deceleration period occurred at approximately the same time after mixing when activated with any of the doses of sodium metasilicate studied here; this behavior was surprisingly insensitive to activator dose. However, this can be related to the importance of the release of Mg^{2+} from the slag in defining the precipitation of the reaction products as this cation interacts and forms reaction products with dissolved aluminates, not with the silicate species supplied by the activator. The pH is sufficiently high to induce extensive slag glass dissolution for all activator compositions tested here (see below), so the differences in heat release peak timing are related directly to the differences in reaction product precipitation times. Thermodynamic modeling has shown that, in general, the C-(N)-A-S-H type gels forming in alkali-activated slag cements precipitate at a much lower extent of slag reaction than the other product phases such as LDHs and/or zeolites [17]. Consequently, it is likely that this type of gel is precipitating during the first stage of the acceleration/deceleration peak identified in the heat release

curves, particularly for lower-Mg slags. The latter stage of the acceleration/deceleration peak is therefore able to be associated with the precipitation of Mg-Al LDH phases.

The heat release curves for slags M06, M07, M08, and M14 activated with 8 wt.% sodium metasilicate are shown in Figure 1D. At this activator dose, the length of the induction period and the length of the acceleration/deceleration period in each sample increases with increasing slag MgO content; the exact inverse of the relationship observed at the lowest activator dose in Figure 1A. However, the results in Figure 1D are consistent with previous observations of decreased reaction kinetics with increasing slag MgO content [9,15], which were obtained at similarly high activator doses. The relative rates of the reaction of the different slags are governed by the alkalinity and soluble silicate concentration supplied by the activator; as noted above, sample M14 reacted quickly in the presence of moderate alkali and soluble silicate concentrations (3 wt.% dose), but was not accelerated significantly in the presence of high alkali and soluble silicate concentrations.

The cumulative heat release curves for all samples are shown in Figure 2. The induction period corresponded to the relatively flat regions at the early stages of the reaction in the cumulative heat release curves. At an activator dose of 3 wt.% sodium metasilicate (Figure 2A), increasing MgO content resulted in increased cumulative heat release during the first 100 h of reaction, indicating that increased MgO content resulted in a greater extent of reaction at this activator dosage if it is assumed that the dissolution heat of the slag glass (defined on a mass basis) is not strongly dependent on its composition and thermal history within the group of slags studied here. There is a relatively weak dependence of aluminosilicate glass and mineral enthalpy of formation on the Mg–Ca substitution [24], and little other systematic information is available for glasses as complex as blast furnace slag, so this assumption is probably acceptable.

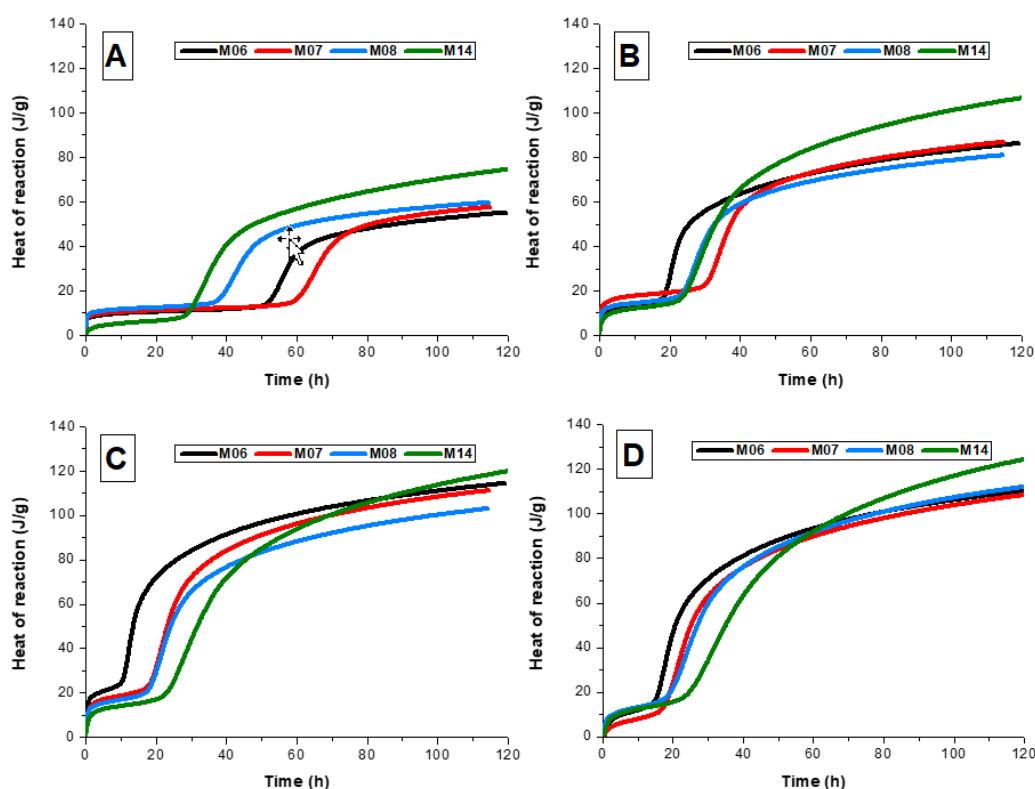


Figure 2. Cumulative heat of reaction of sodium metasilicate activated slag cements produced with activator doses of (A) 3 wt.%, (B) 5 wt.%, (C) 7 wt.%, and (D) 8 wt.% (relative to anhydrous slag), as a function of the slag chemistry.

There was no clear systematic trend in heat release as a function of activator dose and MgO content among M06, M07, and M08 at higher alkali doses (Figure 2B–D). A large increase in slag MgO content

(i.e., sample M14) resulted in higher cumulative heat release at all activator doses, indicating that a high-MgO slag reached a higher reaction extent overall, particularly at lower activator doses. However, the cumulative heat release data show a marked dependence on the activator dose for this slag, unlike the acceleration onset time data (Figure 1), which were relatively insensitive to activator dose.

Independent of slag chemical composition or fineness, an increase in the activator dose of up to 7 wt.% sodium metasilicate (Figure 2A–C) showed a higher cumulative heat release at 100 h. Additionally, previous observations have shown that an increased sodium silicate modulus ($\text{SiO}_2/\text{Na}_2\text{O}$ ratio) results in a greater cumulative heat release [25]. Together, these trends indicate that greater availability of soluble silica in the reaction mixture up to 7 wt.% sodium metasilicate increased the extent of the reaction, most likely by accelerating the generation of conditions that are supersaturated with respect to C-A-S-H, thus increasing the driving force for slag dissolution.

3.2. Correlating Slag Chemistry and Reaction Kinetics

A similar approach to that reported by Winnefeld et al. [26] was adopted in this study to identify any potential correlation between the chemical composition of the slag, the initial precipitation of the reaction products, and the extent of the reaction of the slag. This considers the quality moduli for slag glasses reported by Smolczyk [27] including the formula that is now used in the standard EN 197-1 [28], where each modulus is a different chemical ratio calculated according to various approaches to define the basicity of each slag according to the ratio of network modifying atoms (Ca, Mg, Al) to network forming atoms (Si, Al) (Equations (1)–(4)), where the key difference between the various formulae is the assumption that is made regarding the fraction of Al which acts as either a network modifier or a network former. The correlations between slag composition (represented by the moduli in Equations (1)–(4), and also by slag MgO and Al_2O_3 content) and the cumulative heat of reaction and maximum rate of reaction of the acceleration period, are reported in Figures 3 and 4, respectively, as a function of activator dose.

$$k_3 = \frac{\text{CaO} + \text{MgO}}{\text{SiO}_2} \quad (1)$$

$$k_4 = \frac{\text{CaO} + \text{MgO}}{\text{SiO}_2 + 0.5\text{Al}_2\text{O}_3} \quad (2)$$

$$k_5 = \frac{\text{CaO} + \text{MgO} + \frac{1}{3}\text{Al}_2\text{O}_3}{\text{SiO}_2 + \frac{2}{3}\text{Al}_2\text{O}_3} \quad (3)$$

$$k_7 = \frac{\text{CaO} + \text{MgO} + \text{Al}_2\text{O}_3}{\text{SiO}_2} \quad (4)$$

Figures 3 and 4 show that none of these slag quality coefficients were particularly effective in predicting reactivity under alkali-activation conditions; it is evident that factors other than those captured by the simple chemical moduli actually determine the extent (Figure 3), and particularly the rate (Figure 4) of reaction of the slag. Figure 3 shows that the extent of the reaction is largely insensitive to the quality coefficients within the range studied here, k_3 and k_4 are probably the closest to giving a uniform trend across all slags and activator doses, but the relationship seems relatively weak, and for k_4 , the range of values spanned by this set of slags (which did differ quite significantly in composition and reactivity) was unsatisfactorily low for this to be considered as a useful parameter in the selection of slags for use in alkali-activation. Similarly, neither the MgO content or Al_2O_3 content showed a direct, monotonic correlation with either the cumulative heat release or peak heat release rate.

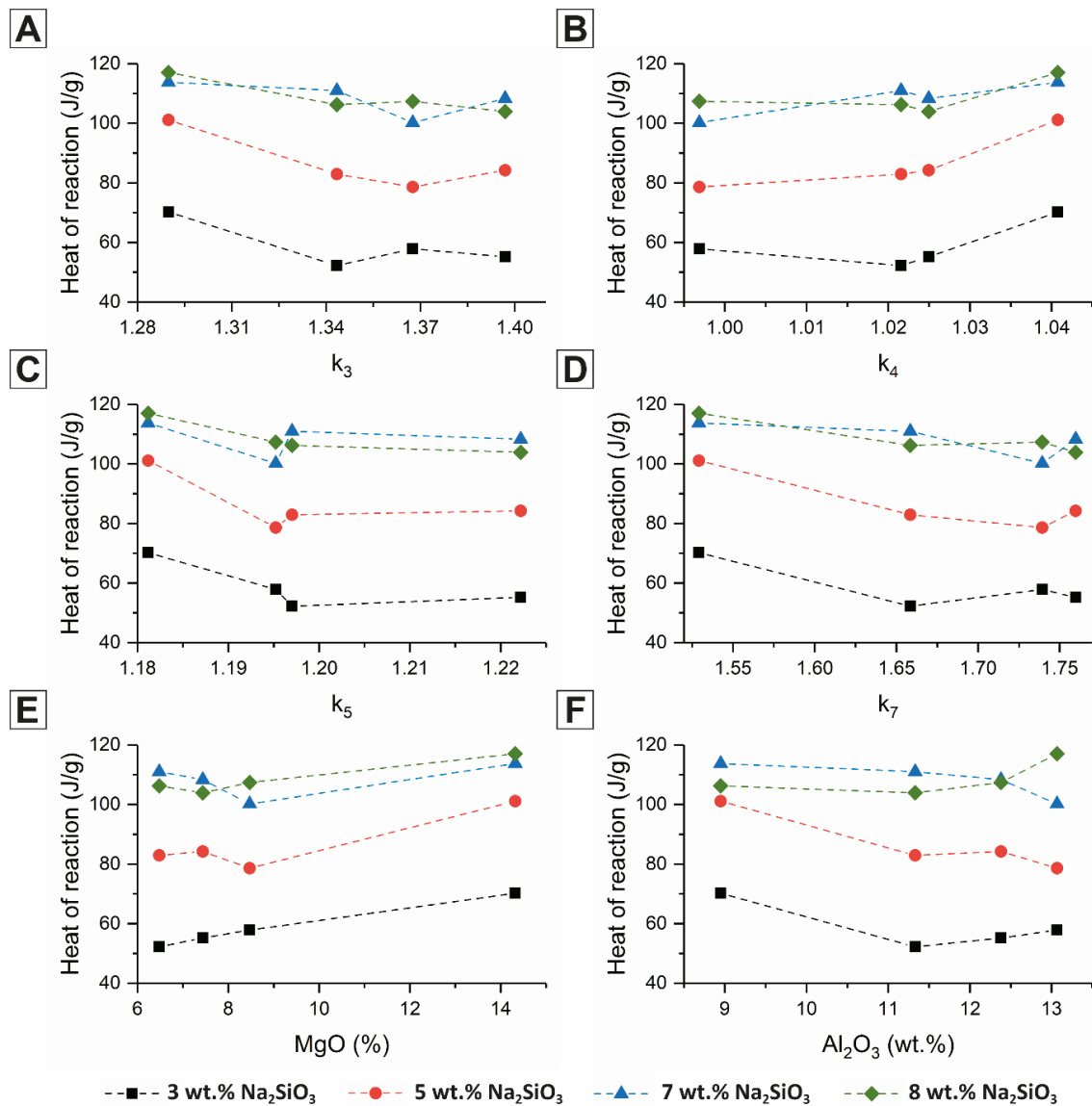


Figure 3. Correlation between the cumulative heat of reaction at 100 h and the quality moduli (A) k_3 , (B) k_4 , (C) k_5 , (D) k_7 , (E) MgO wt.%, and (F) Al₂O₃ wt.% within the slag, for sodium metasilicate activated slag cements produced with different activator concentrations as marked. Dashed lines are shown to guide the eye.

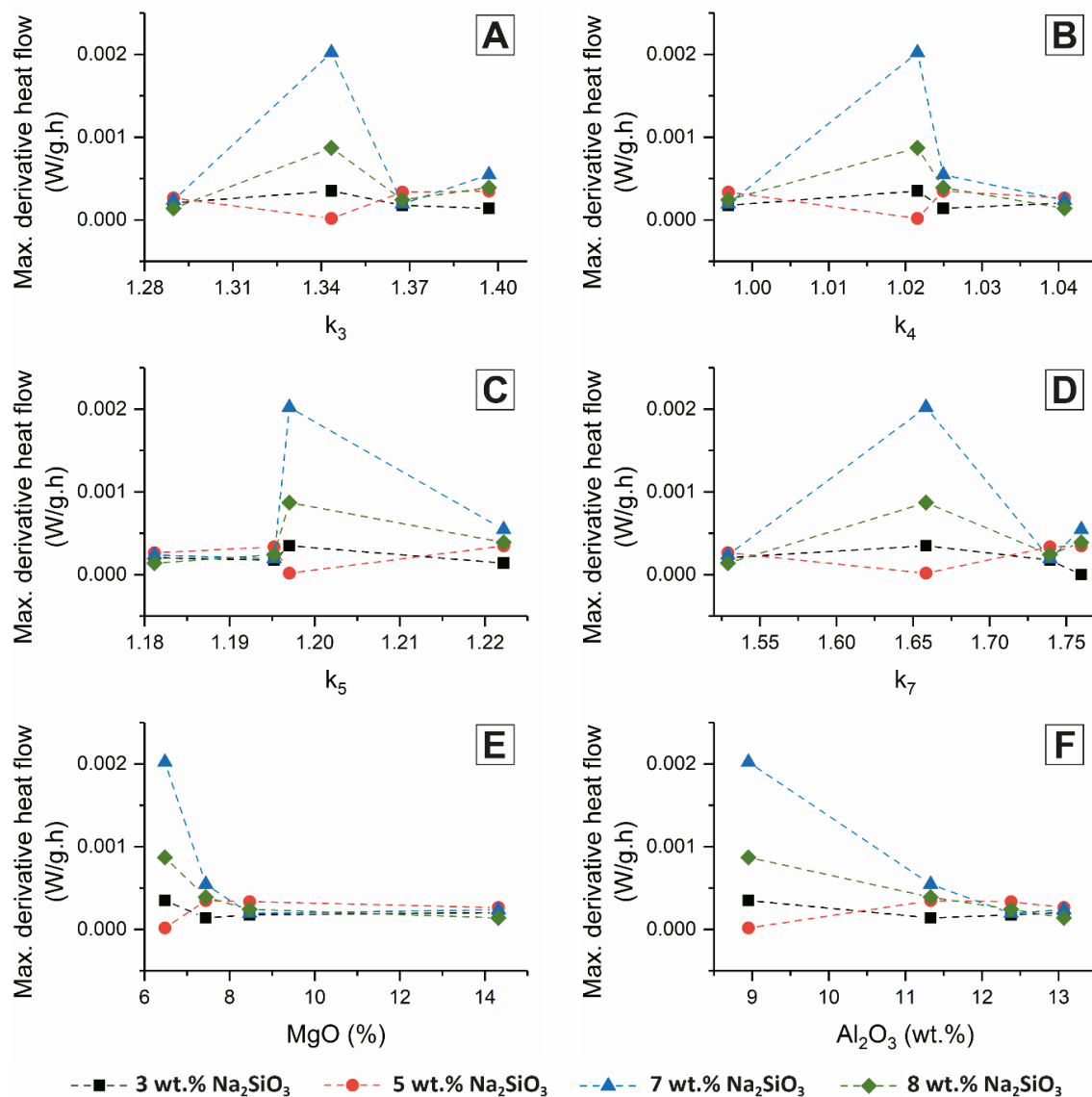


Figure 4. Correlation between the maximum acceleration rate of the reaction (determined from the maximum in the derivative of the heat flow curve) during the acceleration period of the heat release curves, and quality moduli (A) k_3 , (B) k_4 , (C) k_5 , (D) k_7 , (E) MgO wt.%, and (F) Al₂O₃ wt.% within the slag, and for sodium metasilicate activated slag cements produced with different activator concentrations as marked. Dashed lines are shown to guide the eye.

The correlations between the activator dosage and the cumulative heat of the reaction period are shown in Figure 5.

For samples M06, M07, and M08, the cumulative heat of reaction after 100 h increased approximately linearly with increasing activator dosage up to 7 wt.% sodium metasilicate (Figure 5), indicating that within this range, an increased concentration of soluble silicate in the reaction mixture promoted a greater extent of reaction. Increasing the activator dosage from 7 wt.% to 8 wt.% slightly reduced the extent of the reaction for samples M06 and M07, although it continued to increase the extent of reaction for sample M08, and to a lesser degree M14; the slag MgO content seemed to influence the reaction process at high activator doses (>7 wt.%).

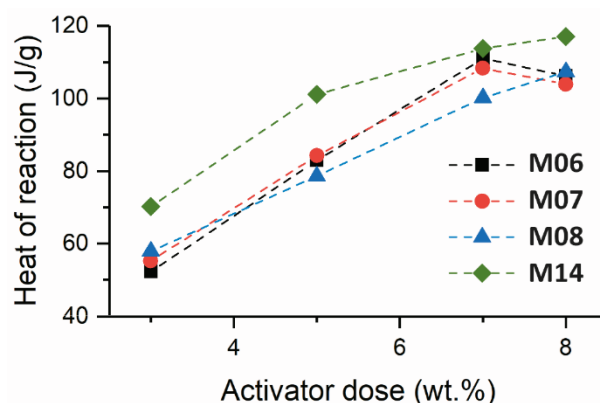


Figure 5. Correlation between Na_2SiO_3 dose (wt.%) and the cumulative heat of reaction at 100 h for sodium metasilicate activated slag cements.

3.3. Influence of Activator Dose in Phase Assemblage Evolution

Figure 6 shows the evolution of the phase assemblage of slag M06 with two different alkali doses as a function of time. Congruent dissolution of slag was assumed as the initial alkalinity of the system would be much higher than pH 12 [29]. The time steps used in the modeling were in accordance with the isothermal calorimetry data as discussed in Section 3.1, while the degree of reaction at each time step was in proportion to the total heat release (Figure 2).

The main reaction products simulated were alkali-substituted calcium aluminate silicate hydrate (C-(N)-A-S-H) gel, strätlingite, hydrotalcite-like phases, and natrolite, similar to the simulation results reported by Myers et al. [17], which matched the experimental observations from previous studies using a subset of these slags at a single activator dose [9,19]. Some transient brucite formation was predicted at the higher activator dose; it is unclear whether this will happen in reality as this phase has not been reported experimentally at an early age in such binders as it may be an artifact due to the assumption of congruent slag dissolution and/or the absence of kinetic limitations on phase formation in the calculations here. The C-(N)-A-S-H gel was the main reaction product in both simulations, regardless of the degree of reaction achieved. The bulk gel chemical compositions are controlled mostly by the availability of CaO , SiO_2 , and Al_2O_3 [30,31], which in practice relate to the chemistry of the slag used, the activator dose, and the degree of reaction achieved. When a higher dose of sodium metasilicate was used (Figure 6C,D), the Ca/Si ratio of the simulated C-(N)-A-S-H gel was reduced due to the higher initial silica content, however this effect was less marked as the degree of reaction of the slag increased because the silica supplied by the slag became dominant. This explained the lower (<1) ratio of Ca/Si shown in Figure 6D before reaching the highest heat of the reaction. The hydrotalcite-like phases were the main secondary phases that formed in this slag upon activation, the formation of which is closely related to the MgO content in the slag [9] as well as the availability of Al species in the aqueous phase (Figure 7).

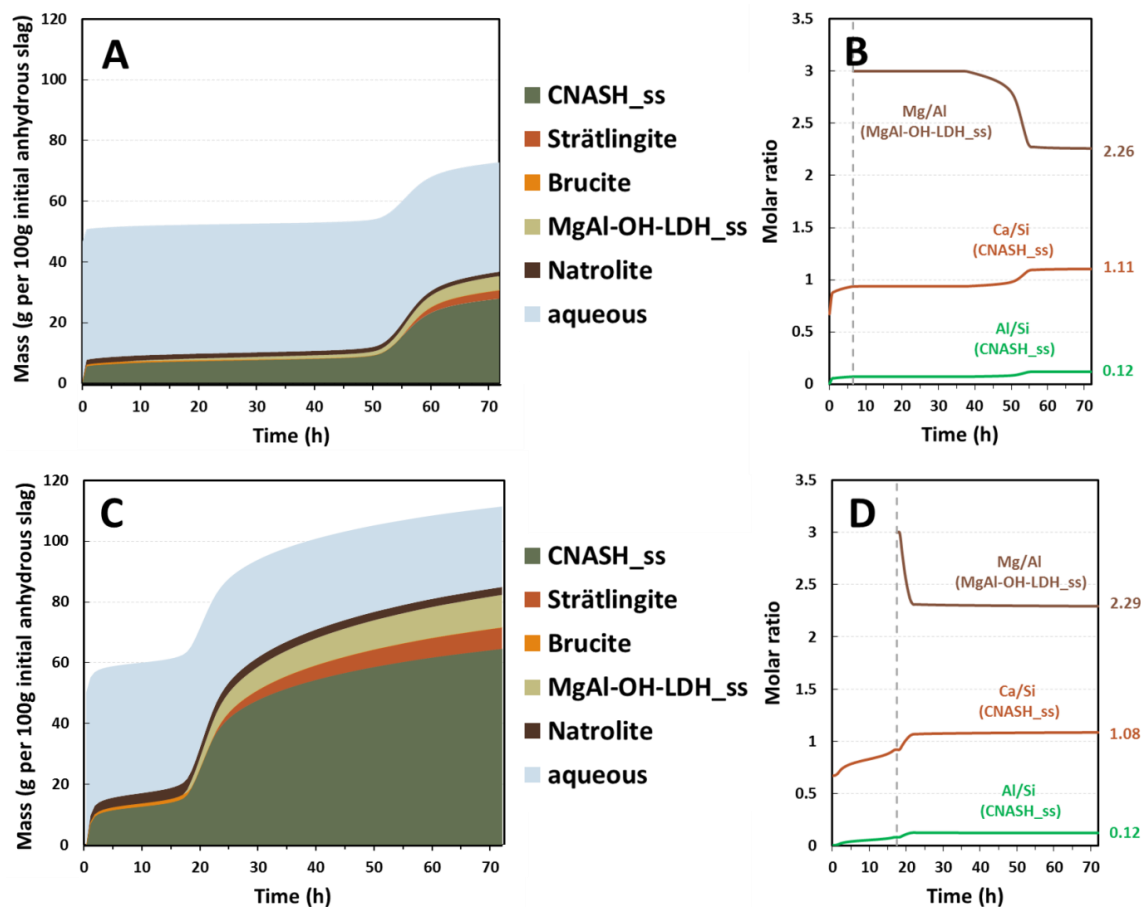


Figure 6. Phase assemblage simulations of sodium metasilicate-activated slag as a function of time. (A) Slag M06 activated with 3 wt.% sodium silicate activator, and (B) corresponding molar ratios of the main components in the solid solutions CNASH_{ss} and MgAl-OH-LDH_{ss}. (C) Slag M06 activated with 7 wt.% sodium silicate activator, and (D) corresponding molar ratios of the main component in the solid solution CNASH_{ss} and MgAl-OH-LDH_{ss}. The mass of unreacted slag is not shown.

Figure 7 shows the compositions of the aqueous constituents shown in Figure 6; Figure 7A corresponds to Figure 6A, and Figure 7B to Figure 6C. In each case, the pH was above 13 but decreased with time; the pH of these alkali-activated slag binders in the fresh state was within the same range as the pH developed by the hydration of plain Portland cement, and so should not be viewed as unusually or inappropriately high for the general usage of alkali-activated slag as a cement. The concentrations of dissolved ions in this thermodynamic simulation are determined by equilibrium with the precipitated solid phase assemblage at each point in time, so after the initial rapid reaction (which removes much of the Si from solution), these concentrations change only slowly until there is a shift in the makeup of the phase assemblage that then generates a rapid re-equilibration of the pore solution (e.g., at 52 h in Figure 7A, just before 20 h in Figure 7B). It is notable that the dissolved sulfur concentrations remain high throughout the reaction process; this element is present in reduced form (HS^-), which is not readily incorporated into any of the solid phases within the database used, and so remains free in solution.

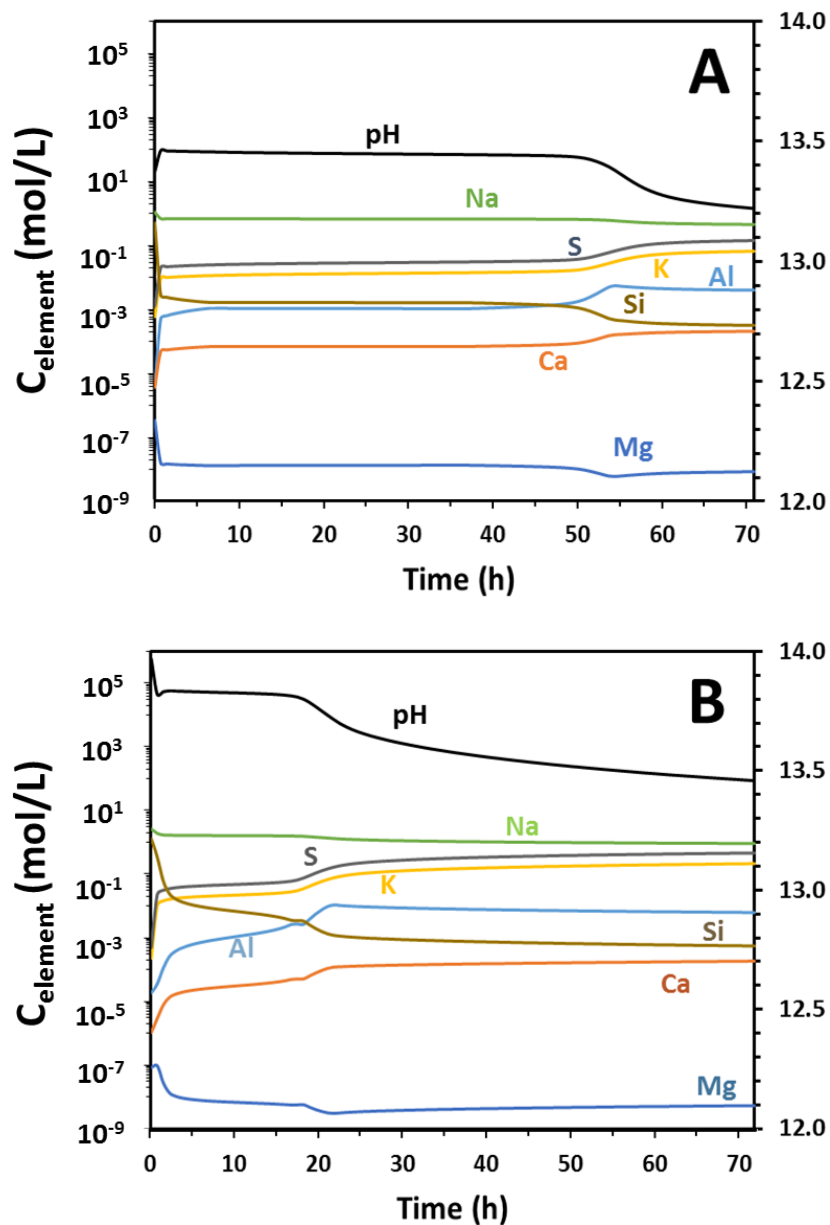


Figure 7. Concentrations of elements in the aqueous phase (pore solution) of (A) M06 with 3 wt.% sodium silicate activator, and (B) M06 with 7 wt.% sodium silicate activator, as a function of time.

4. Conclusions

Slight differences in slag chemistry induce notable changes in the reaction kinetics of silicate-activated slag cements, as a function of the activator dose. This is consistent with the scattered literature available reporting differences in the optimized activation conditions when varying the slag source. Although small differences in the particle size distribution were identified in all the slags assessed, the soluble silicate concentration influenced the reaction kinetics in different ways depending on the slag composition. Highly soluble silicate concentrations delayed formation of the Mg–Al LDH phases in these cements, particularly in slags with reduced CaO content and high MgO. Overall, this delays the kinetics of reaction; however, it does not seem to impact the degree of reaction significantly at 100 h after mixing.

The kinetics of reaction identified in the sodium silicate activated slag cements were consistent with the fact that preferential formation of C-(A)-S-H type gels prevailed, which reduced the concentration of Al available in the system, and hindered the formation of Mg–Al LDH phases

during the early stages of reaction. A clear correlation between the quality moduli and the kinetics of reaction of silicate-activated slag cements was not identified; however, a clear relationship between the Al_2O_3 and MgO contents within the slag and the kinetics of reaction was observed for most of the slags tested. This elucidates that the reaction kinetics of these systems is strongly dependent on the Al_2O_3 content in the slag and the dissolution rates of CaO and MgO at high alkali concentrations, as this controls the phase assemblage development in these cements. Independent of slag chemical composition or fineness, an increasing activator dose of up to 7 wt.% sodium metasilicate promoted greater cumulative heat release after 100 h, and no significant differences were identified at higher activator doses. Hence, this activator dose seems to be the upper limit of effectiveness of the activator in silicate-activated slag cements.

Author Contributions: Conceptualization, S.A.B. and J.L.P.; Funding acquisition, J.L.P. and S.A.B.; Investigation, M.C., B.W., and X.K.; Methodology, S.A.B. and J.L.P.; Project administration, S.A.B.; Supervision, J.L.P. and S.A.B.; Writing—original draft, M.C.; Writing—review & editing, B.W., X.K., J.L.P., and S.A.B.

Funding: This research was funded in part by the European Research Council under the European Union's Seventh Framework Program (FP7/2007–2013)/ERC Grant Agreement #335928 (GeopolyConc), and in part by the Engineering and Physical Sciences Research Council (EP/P013171/1). Participation of SAB in this study was sponsored by EPSRC through ECF EP/R001642/1.

Acknowledgments: The technical support provided by Oday Hussein in collecting some of the calorimetry data, and the donation of the slags by ECOCEM and by Joséé Duchesne (Université Laval, Canada) is gratefully acknowledged.

Conflicts of Interest: The authors declare no conflict of interest.

References

- Snellings, R. Assessing, understanding and unlocking supplementary cementitious materials. *RILEM Tech. Lett.* **2016**, *1*, 50–55. [[CrossRef](#)]
- Provis, J.L.; Bernal, S.A. Geopolymers and related alkali-activated materials. *Annu. Rev. Mater. Res.* **2014**, *44*, 299–327. [[CrossRef](#)]
- Provis, J.L. Geopolymers and other alkali activated materials: Why, how, and what? *Mater. Struct.* **2014**, *47*, 11–25. [[CrossRef](#)]
- Provis, J.L.; Palomo, A.; Shi, C. Advances in understanding alkali-activated materials. *Cem. Concr. Res.* **2015**, *78*, 110–125. [[CrossRef](#)]
- Wang, S.D.; Scrivener, K.L.; Pratt, P.L. Factors affecting the strength of alkali-activated slag. *Cem. Concr. Res.* **1994**, *24*, 1033–1043. [[CrossRef](#)]
- Wang, S.-D.; Scrivener, K.L. ^{29}Si and ^{27}Al NMR study of alkali-activated slag. *Cem. Concr. Res.* **2003**, *33*, 769–774. [[CrossRef](#)]
- Puertas, F.; Fernández-Jiménez, A.; Blanco-Varela, M.T. Pore solution in alkali-activated slag cement pastes. Relation to the composition and structure of calcium silicate hydrate. *Cem. Concr. Res.* **2004**, *34*, 139–148. [[CrossRef](#)]
- Ben Haha, M.; le Saout, G.; Winnefeld, F.; Lothenbach, B. Influence of activator type on hydration kinetics, hydrate assemblage and microstructural development of alkali activated blast-furnace slags. *Cem. Concr. Res.* **2011**, *41*, 301–310. [[CrossRef](#)]
- Bernal, S.A.; Nicolas, R.S.; Myers, R.J.; Mejía de Gutiérrez, R.; Puertas, F.; van Deventer, J.S.J.; Provis, J.L. MgO content of slag controls phase evolution and structural changes induced by accelerated carbonation in alkali-activated binders. *Cem. Concr. Res.* **2014**, *57*, 33–43. [[CrossRef](#)]
- Provis, J.L.; van Deventer, J.S.J. (Eds.) *Geopolymers: Structures, Processing, Properties and Industrial Applications*; Woodhead: Cambridge, UK, 2009; 448p.
- Fernández-Jiménez, A.; Puertas, F. Effect of activator mix on the hydration and strength behaviour of alkali-activated slag cements. *Adv. Cem. Res.* **2003**, *15*, 129–136. [[CrossRef](#)]
- Song, S.; Sohn, D.; Jennings, H.M.; Mason, T.O. Hydration of alkali-activated ground granulated blast furnace slag. *J. Mater. Sci.* **2000**, *35*, 249–257. [[CrossRef](#)]
- Zhou, H.; Wu, X.; Xu, Z.; Tang, M. Kinetic study on hydration of alkali-activated slag. *Cem. Concr. Res.* **1993**, *23*, 1253–1258.

14. Osborn, E.F.; Roeder, P.L.; Ulmer, G.C. Part I—Phase equilibria at solidus temperatures in the quaternary system CaO-MgO-Al₂O₃-SiO₂ and their bearing on optimum composition of blast furnace slag and on slag properties. In *Bulletin of the Earth and Mineral Sciences Experiment Station*; The Pennsylvania State University: State College, PA, USA, 1969.
15. Ben Haha, M.; Lothenbach, B.; le Saout, G.; Winnefeld, F. Influence of slag chemistry on the hydration of alkali-activated blast-furnace slag—Part I: Effect of MgO. *Cem. Concr. Res.* **2011**, *41*, 955–963. [[CrossRef](#)]
16. Ben Haha, M.; Lothenbach, B.; le Saout, G.; Winnefeld, F. Influence of slag chemistry on the hydration of alkali-activated blast-furnace slag—Part II: Effect of Al₂O₃. *Cem. Concr. Res.* **2012**, *42*, 74–83. [[CrossRef](#)]
17. Myers, R.J.; Lothenbach, B.; Bernal, S.A.; Provis, J.L. Thermodynamic modelling of alkali-activated slag cements. *Appl. Geochem.* **2015**, *61*, 233–247. [[CrossRef](#)]
18. Myers, R.J.; Bernal, S.A.; Provis, J.L. A thermodynamic model for C-(N-)A-S-H gel: CNASH_{ss}. Derivation and validation. *Cem. Concr. Res.* **2014**, *66*, 27–47. [[CrossRef](#)]
19. Myers, R.J.; Bernal, S.A.; Gehman, J.D.; van Deventer, J.S.J.; Provis, J.L. The role of Al in cross-linking of alkali-activated slag cements. *J. Am. Ceram. Soc.* **2014**, *98*, 996–1004. [[CrossRef](#)]
20. Shi, C.; Day, R.L. A calorimetric study of early hydration of alkali-slag cements. *Cem. Concr. Res.* **1995**, *25*, 1333–1346. [[CrossRef](#)]
21. Frankel, G.S.; Vienna, J.D.; Lian, J.; Scully, J.R.; Gin, S.; Ryan, J.V.; Wang, J.; Kim, S.H.; Windl, W.; Du, J. A comparative review of the aqueous corrosion of glasses, crystalline ceramics, and metals. *NPJ Mater. Degrad.* **2018**, *2*, 15. [[CrossRef](#)]
22. Shi, C.; Day, R.L. Some factors affecting early hydration of alkali-slag cements. *Cem. Concr. Res.* **1996**, *26*, 439–447. [[CrossRef](#)]
23. Bernal, S.A.; Provis, J.L.; Mejía de Gutierrez, R.; Rose, V. Evolution of binder structure in sodium silicate-activated slag-metakaolin blends. *Cem. Concr. Compos.* **2011**, *33*, 46–54. [[CrossRef](#)]
24. Navrotsky, A.; Tian, Z.-R. Systematics in the enthalpies of formation of anhydrous aluminosilicate zeolites, glasses, and dense phases. *Chem.—Eur. J.* **2001**, *7*, 769–774. [[CrossRef](#)]
25. Gebregziabihier, B.S.; Thomas, R.J.; Peethamparan, S. Temperature and activator effect on early-age reaction kinetics of alkali-activated slag binders. *Constr. Build. Mater.* **2016**, *113*, 783–793. [[CrossRef](#)]
26. Winnefeld, F.; Ben Haha, M.; le Saout, G.; Costoya, M.; Ko, S.-C.; Lothenbach, B. Influence of slag composition on the hydration of alkali-activated slags. *J. Sustain. Cem.-Based Mater.* **2014**, *4*, 85–100. [[CrossRef](#)]
27. Smolczyk, H.G. Slag structure and identification of slags. In *Proceedings of the 7th International Congress on the Chemistry of Cement*, Paris, France, 30 June–4 July 1980.
28. European Committee for Standardization (CEN). *Cement—Part 1: Composition, Specifications and Conformity Criteria for Common Cements (EN 197-1)*; European Committee for Standardization (CEN): Brussels, Belgium, 2011.
29. Snellings, R. Surface chemistry of calcium aluminosilicate glasses. *J. Am. Ceram. Soc.* **2015**, *98*, 303–314. [[CrossRef](#)]
30. Macphee, D.E.; Luke, K.; Glasser, F.P.; Lachowski, E.E. Solubility and aging of calcium silicate hydrates in alkaline solutions at 25 °C. *J. Am. Ceram. Soc.* **1989**, *72*, 646–654. [[CrossRef](#)]
31. L'Hôpital, E.; Lothenbach, B.; le Saout, G.; Kulik, D.; Scrivener, K. Incorporation of aluminium in calcium-silicate-hydrates. *Cem. Concr. Res.* **2015**, *75*, 91–103. [[CrossRef](#)]

